

Time-dependent numerical renormalization group method for multiple quenches: towards exact results for the long time limit of thermodynamic observables and spectral functions

H. T. M. Nghiem^{1,2} and T. A. Costi¹

¹*Peter Grünberg Institut and Institute for Advanced Simulation, Research Centre Jülich, 52425 Jülich, Germany*

²*Advanced Institute for Science and Technology, Hanoi University of Science and Technology, 10000 Hanoi, Vietnam*

(Dated: July 15, 2022)

We develop an alternative time-dependent numerical renormalization group formalism (TDNRG) for multiple quenches and implement it to study the response of a quantum impurity system to a general pulse. Within this approach, we reduce the contribution of the NRG approximation to numerical errors in the time evolution of observables by a formulation that uses the difference of eigenvalues instead of their absolute values, as in our previous multiple-quench TDNRG formalism [Nghiem *et al.*, Phys. Rev. B **89**, 075118 (2014); Phys. Rev. B **90**, 035129 (2014)]. We demonstrate that the new formalism yields a smaller cumulative error in the trace of the projected density matrix as a function of time and a smaller discontinuity of local observables between quenches than in our previous approach [Nghiem *et al.*, Phys. Rev. B **90**, 035129 (2014)]. Moreover, by increasing the switch-on time, the time between the first and last quench of the discretized pulse, the long time limit of observables systematically converges to its expected value in the final state, i.e., the more adiabatic the switching, the more accurately is the long time limit recovered. The present formalism can be straightforwardly extended to infinite switch-on times. We show that this yields highly accurate results for the long time limit of both thermodynamic observables and spectral functions, and overcomes the significant errors within the single quench formalism [Anders *et al.*, Phys. Rev. Lett. **95**, 196801 (2005); Nghiem *et al.*, Phys. Rev. Lett. **119**, 156601 (2017)]. This improvement provides a first step towards an accurate description of nonequilibrium steady states of quantum impurity systems, e.g., within the scattering states NRG approach [Anders, Phys. Rev. Lett. **101**, 066804 (2008)].

PACS numbers: 75.20.Hr, 71.27.+a, 72.15.Qm, 73.63.Kv

I. INTRODUCTION

The response of strongly correlated quantum impurity systems to quenches, pulses, static and time-dependent fields, remains a challenging theoretical topic of relevance to a number of fields, including, low energy ion-surface scattering^{1,2}, time dependent dynamics and pumping in quantum dots^{3–6}, pump-probe spectroscopies of correlated electron materials^{7–10}, and to proposed cold atom realizations of Anderson and Kondo impurities^{11–14} probed in the time domain¹⁵.

Techniques currently being used to investigate the time-dependent dynamics of quantum impurity systems, include functional and real-time renormalization group methods^{16–18}, flow equation^{19,20}, quantum Monte Carlo^{21–24}, and density matrix renormalization group methods^{25–27}, the hierarchical quantum master equation approach^{28,29}, and the time-dependent numerical renormalization group (TDNRG) method^{30–39}. However, no single technique is able to address in a nonperturbative and numerically exact way the time-dependent and nonequilibrium dynamics of quantum impurity systems in the interesting low temperature strong coupling regime. For example, quantum Monte Carlo approaches become numerically expensive in the zero temperature limit²², the functional renormalization group approach, while versatile, is often only quantitatively accurate for weak to intermediate interaction strengths^{16,40} and the (single-quench) TDNRG approach suffers from imperfect thermalization and finite errors in the long time limit due, primarily, to the use a logarithmic discretization of the bath^{31–34,36–39,41}. Nevertheless, the latter technique remains promising since it is based on Wilson’s (equilibrium) numerical renormalization group

method^{42–45}, which, by construction, is nonperturbative, and highly suited for accessing the low temperature strong coupling physics of quantum impurity models. A main aim of the present paper will be to further develop the TDNRG, in its multiple-quench version^{36,37}, towards an accurate calculation of thermodynamic observables and spectral functions in the long time limit, thereby overcoming the above mentioned limitations of the single quench TDNRG. While the previous multiple quench TDNRG approach^{36,37} already provides an improvement over the single quench TDNRG, it also suffers from a number of problems, which we outline below, and which we overcome with the present formulation.

In a previous multiple quench TDNRG formalism for general pulses, in which the pulse was discretized into a sequence of quenches, we identified several problems associated with the use of the NRG approximation in the time evolution of observables³⁷ (to be described in more detail in Secs. II–III); (i), the trace of the projected density matrix was found to deviate increasingly away from 1 with increasing switch-on time $\tilde{\tau}_n$, the time required to switch from the initial to the final state, up to some finite switch-on time, before decreasing again for longer switch-on times (with a maximum deviation, however, below 1%), (ii), the time evolution of an observable exhibited small discontinuities at the times corresponding to all but the first quench. Similar errors have been found within a hybrid TDNRG approach to periodic switching³⁴. We also investigated within the above approach, the dependence of the long time limit of observables $O(t \rightarrow \infty)$ on the switch on time, $\tilde{\tau}_n$, finding convergence of this towards the exact long time limit in the final state for sufficiently large $\tilde{\tau}_n$ (i.e., for sufficiently slow, or adiabatic, switching). By contrast, a single-quench

calculation (for the same initial and final states) yields a significantly less accurate long time limit $O(t \rightarrow \infty)$. While the above suggests a systematic way of improving the long time limit of observables, in practice, $O(t \rightarrow \infty)$ versus $\tilde{\tau}_n$ converged non-monotonically to its correct long time limit within the approach of Refs. 36 and 37 and there was no easy way within this formalism to extract, other than numerically, the desired limit $\tilde{\tau}_n \rightarrow \infty$ (and hence the $t \rightarrow \infty$ limit).

In this paper, we present an alternative TDNRG formalism for multiple quenches which, to a large extent, overcomes the above problems, namely, (i), the trace of the projected density matrix versus $\tilde{\tau}_n$ remains significantly closer to 1 for all $\tilde{\tau}_n$, (ii), observables exhibit significantly smaller discontinuities after each quench, and, (iii), the limit of infinite switch-on times can be taken analytically within this formalism and allows obtaining the long time limit of thermodynamic observables with high accuracy.

Extending this formalism to spectral functions, we also recover the expected long time value of the spectral function in the equilibrium final state with high accuracy. Within a scattering states approach to nonequilibrium steady states^{32,33}, such a calculation would allow the low temperature nonequilibrium steady state spectral function and conductance of interacting quantum dots to be calculated accurately for arbitrary bias and gate voltages. Besides the relevance of this for experiments on quantum dots^{46–48}, it would also go beyond the recent exact Fermi liquid approach which addresses only the low bias voltage regime (relative to the Kondo scale)⁴⁹.

The outline of the paper is as follows: In section II, the alternative multiple quench TDNRG formalism is derived for finite switch on times to reduce the effect of the NRG approximation by only using the difference of eigenvalues instead of their absolute values as in Ref. 36 and 37. The improvement is shown by comparing calculations from the two formalisms for the resonant level model and the Anderson impurity model in Sec. III. In section IV, the (straight forward) extension to infinite switch-on times is derived from the formalism presented in Sec. II. Applications are made to the long time limit of the spectral function in Sec. IV A and to thermodynamic observables (occupation and double occupation) in Sec. IV B with comparison of the results to the their expected values in the equilibrium final state. In addition, we show in Sec. IV C results for the occupation number of the resonant level model calculated within exact diagonalization (ED) for multiple quenches in the infinite switch-on time limit, which further support the conclusions made with the multiple quench TDNRG formalism. The TDNRG expression for the spectral function for multiple quenches, for a finite and infinite switch-on time, is derived in Appendix A. Results for the switch-on time dependence of the spectral function are presented in Appendix B. Finally, Appendix C presents the generalization of ED to study the time evolution of a system following multiple quenches with both finite and infinite switch-on times.

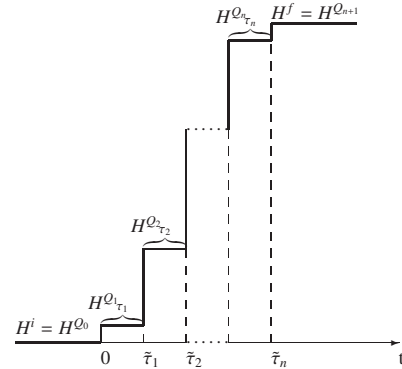


FIG. 1. A system driven from an initial to a final state via a sequence of quantum quenches at times $\tilde{\tau}_0 = 0, \tilde{\tau}_1, \dots, \tilde{\tau}_n$ with evolution according to $\{H^{Q_p}\}$ in the time step $\tilde{\tau}_{p-1} \leq t < \tilde{\tau}_p$ with $H^{Q_0} = H^i$ and $H^{Q_{n+1}} = H^f$. The time, $\tilde{\tau}_n = \sum_{p=1}^n \tau_p$, to switch from H^i to H^f via the sequence of quantum quenches will be called the switch-on time (or, equivalently the pulse duration).

II. MULTIPLE QUENCH TDNRG FOR GENERAL PULSES: ALTERNATIVE FORMALISM

We consider a system driven from an initial state (described by H^i) to a final state (described by H^f) in a time interval $[0, \tilde{\tau}_n]$ via a sequence of $n+1$ quantum quenches described by H^{Q_p} , $p = 1, \dots, n+1$, switched on at times $\tilde{\tau}_{p-1}$, $p = 1, \dots, n+1$ (with $\tilde{\tau}_0 = 0$) and having duration τ_p (except for $H^{Q_{p=n+1}} = H^f$ which acts for all $t > \tilde{\tau}_n$) as depicted in Fig. 1. The time to switch from the initial to the final state, $\tilde{\tau}_n$, will be referred to as the switch-on time throughout the paper (equivalently, this can be called the duration of the pulse).

The Hamiltonians, H^{Q_p} , $p = 1, \dots, n+1$, will represent an Anderson impurity model $H(t)$ for $\tilde{\tau}_{p-1} \leq t < \tilde{\tau}_p$, with

$$H(t) = H_{\text{imp}} + H_{\text{bath}} + H_{\text{int}}.$$

Here, $H_{\text{imp}} = \sum_{\sigma} \varepsilon_d(t) n_{d\sigma} + U(t) n_{d\uparrow} n_{d\downarrow}$ describes an impurity with a local level of energy $\varepsilon_d(t)$ and a Coulomb repulsion $U(t)$ between opposite spin electrons in the local level. The impurity interacts with free conduction electrons described by $H_{\text{bath}} = \sum_{k\sigma} \varepsilon_{k\sigma} c_{k\sigma}^{\dagger} c_{k\sigma}$ via a hybridization interaction $H_{\text{int}} = V \sum_{k\sigma} (c_{k\sigma}^{\dagger} d_{\sigma} + h.c.)$. The time dependence enters through either a time dependent level position $\varepsilon_d(t)$ or a time dependent Coulomb repulsion $U(t)$ and will be specified in detail for each switching protocol later. We shall consider a time-independent hybridization V throughout this paper, and we shall denote the constant single-particle broadening of the resonant level by $\Gamma = \pi\rho V^2$, where $\rho = 1/2D$ is the constant density of states per spin of the conduction electrons and $D = 1$ is the half bandwidth.

The quench Hamiltonians, H^{Q_p} , $p = 1, \dots, n+1$, are solved by using Wilson's NRG approach^{43,44} to yield the eigenstates and eigenvalues of each quench Hamiltonian at each NRG iteration $m = m_0, \dots, N$, where N is the longest chain diagonalized and m_0 (typically 6 or 7) is the first iteration at which high energy states are discarded. We make use of the complete basis set of discarded states³⁰ $\{|l_p e_p m_p\rangle_{Q_p}\}$ of H^{Q_p} where

l_p labels the eigenstate, e_p the environment variable and m_p the truncated Hamiltonian at NRG iteration $m = m_p$ and the following decomposition of unity applies

$$\sum_{l_p e_p m_p} |l_p e_p m_p\rangle_{Q_p Q_p} \langle l_p e_p m_p| = 1.$$

In addition, in evaluating thermodynamic expectation values of observables, we used the full density matrix representation⁵⁰ for the initial state density matrix ρ of H^i and the z-averaging procedure^{51,52} to reduce discretization effects.

With the above preliminaries, we can now write down the time evolution $O(t)$ of a local observable \hat{O} at time $t \in [\tilde{\tau}_p, \tilde{\tau}_{p+1})$. In the notation of Ref. 36 and 37 we have

$$O(t) = \sum_{m_{p+1} l_{p+1} e_{p+1}} \mathcal{Q}_{p+1} \langle l_{p+1} e_{p+1} m_{p+1} | e^{-iH^{\mathcal{Q}_{p+1}}(t-\tilde{\tau}_p)} e^{-iH^{\mathcal{Q}_p} \tau_p} \dots e^{-iH^{\mathcal{Q}_1} \tau_1} \\ \times \rho e^{iH^{\mathcal{Q}_1} \tau_1} \dots e^{iH^{\mathcal{Q}_p} \tau_p} e^{iH^{\mathcal{Q}_{p+1}}(t-\tilde{\tau}_p)} \hat{O} | l_{p+1} e_{p+1} m_{p+1} \rangle_{Q_{p+1}}, \quad (1)$$

with ρ the full density matrix⁵⁰ of the initial state Hamiltonian H_i at inverse temperature $\beta = 1/T$. For the simplest case with $\tilde{\tau}_1 > t \geq \tilde{\tau}_0$, the single quench result for $O(t)$ applies³⁰. For the next simplest case with $\tilde{\tau}_2 > t \geq \tilde{\tau}_1$, we have

$$O(t) = \sum_{m_2 l_2 e_2} \mathcal{Q}_2 \langle l_2 e_2 m_2 | e^{-iH^{\mathcal{Q}_2}(t-\tilde{\tau}_1)} e^{-iH^{\mathcal{Q}_1} \tau_1} \\ \times \rho e^{iH^{\mathcal{Q}_1} \tau_1} e^{iH^{\mathcal{Q}_2}(t-\tilde{\tau}_1)} \hat{O} | l_2 e_2 m_2 \rangle_{Q_2} \\ = \sum_{m_2 l_2 e_2} \sum_{m_2' l_2' e_2'} \sum_{m_1 l_1 e_1} \sum_{m_1' l_1' e_1'} \mathcal{Q}_2 \langle l_2 e_2 m_2 | e^{-iH^{\mathcal{Q}_2}(t-\tilde{\tau}_1)} | l_1 e_1 m_1 \rangle_{Q_1} \\ \times \mathcal{Q}_1 \langle l_1 e_1 m_1 | e^{-iH^{\mathcal{Q}_1} \tau_1} \rho e^{iH^{\mathcal{Q}_1} \tau_1} | l_1' e_1' m_1' \rangle_{Q_1} \\ \times \mathcal{Q}_1 \langle l_1' e_1' m_1' | e^{iH^{\mathcal{Q}_2}(t-\tilde{\tau}_1)} | l_2' e_2' m_2' \rangle_{Q_2} \langle l_2' e_2' m_2' | \hat{O} | l_2 e_2 m_2 \rangle_{Q_2},$$

where three decompositions of unity $1 = \sum_{l e m} |l e m\rangle \langle l e m|$ have been employed. Next, we use the identity⁵³

$$\sum_{m_2 l_2 e_2} \sum_{m_2' l_2' e_2'} \sum_{m_1 l_1 e_1} \sum_{m_1' l_1' e_1'} = \sum_m \sum_{e_1 e_1' e_2 e_2'} \sum_{r_1 s_1 r_2 s_2} \quad (2)$$

to convert the multiple-shell sums over the four different Wilson chains in the above expression for $O(t)$ into a single shell-diagonal (restricted) sum involving kept states ($K_1 K_1'$ etc³¹), obtaining

$$O(t) = \sum_m \sum_{r_1 s_1 r_2 s_2} \sum_{e_1 e_1' e_2 e_2'} \mathcal{Q}_2 \langle r_2 e_2 m | e^{-iH^{\mathcal{Q}_2}(t-\tilde{\tau}_1)} | r_1 e_1 m \rangle_{Q_1} \\ \times \mathcal{Q}_1 \langle r_1 e_1 m | e^{-iH^{\mathcal{Q}_1} \tau_1} \rho e^{iH^{\mathcal{Q}_1} \tau_1} | s_1 e_1' m \rangle_{Q_1} \\ \times \mathcal{Q}_1 \langle s_1 e_1' m | e^{iH^{\mathcal{Q}_2}(t-\tilde{\tau}_1)} | s_2 e_2' m \rangle_{Q_2} \langle s_2 e_2' m | \hat{O} | r_2 e_2 m \rangle_{Q_2} \\ = \sum_m \sum_{r_1 s_1 r_2 s_2} S_{r_2 r_1}^m \sum_e \mathcal{Q}_1 \langle r_1 e_1 m | \rho | s_1 e_1 m \rangle_{Q_1} e^{-i(E_{r_1}^m - E_{s_1}^m) \tau_1} \\ \times S_{s_1 s_2}^m O_{s_2 r_2}^m e^{-i(E_{r_2}^m - E_{s_2}^m) (t-\tilde{\tau}_1)} \\ = \sum_m \sum_{r_1 s_1 r_2 s_2} S_{r_2 r_1}^m \rho_m^{i \rightarrow \mathcal{Q}_1}(r_1, s_1) e^{-i(E_{r_1}^m - E_{s_1}^m) \tau_1} \\ \times S_{s_1 s_2}^m O_{s_2 r_2}^m e^{-i(E_{r_2}^m - E_{s_2}^m) (t-\tilde{\tau}_1)}. \quad (3)$$

Here, $S_{r_2 r_1}^m$ is the overlap matrix element which is defined as $S_{r_2 r_1}^m \times \delta_{e_2, e_1} = \mathcal{Q}_2 \langle r_2 e_2 m | r_1 e_1 m \rangle_{Q_1}$, $O_{s_2 r_2}^m$ is the matrix elements of \hat{O} that $O_{s_2 r_2}^m \times \delta_{e_2', e_2} = \mathcal{Q}_2 \langle s_2 e_2' m | \hat{O} | r_2 e_2 m \rangle_{Q_2}$, and $\rho_m^{i \rightarrow \mathcal{Q}_1}(r_1, s_1) = \sum_e \mathcal{Q}_1 \langle r_1 e_1 m | \rho | s_1 e_1 m \rangle_{Q_1}$ is the reduced initial state density matrix (of H_i) projected onto the state of $H^{\mathcal{Q}_1}$. Furthermore, in the second line of Eq. (3), use has been made of the NRG approximation in the form $e^{iH^{\mathcal{Q}_1} \tau_1} | r_1 e_1 m \rangle_{Q_1} \approx e^{iE_{r_1}^m \tau_1} | r_1 e_1 m \rangle_{Q_1}$, which, except in the limit of a vanishing switch-on time $\tau_1 = 0$, incurs a finite error in the time evolution, so Eq. (3) should be understood as being approximate.

For the general case with $t \in [\tilde{\tau}_p, \tilde{\tau}_{p+1})$, we obtain, by using a generalization of Eq. (2)⁵³,

$$O(t) = \sum_m \sum_{r_1 s_1 \dots r_p s_p r_{p+1} s_{p+1}} S_{r_{p+1} r_p}^m \dots S_{r_2 r_1}^m \rho_m^{i \rightarrow \mathcal{Q}_1}(r_1, s_1) \\ \times e^{-i(E_{r_1}^m - E_{s_1}^m) \tau_1} S_{s_1 s_2}^m \dots e^{-i(E_{r_p}^m - E_{s_p}^m) \tau_p} S_{s_p s_{p+1}}^m \\ \times O_{s_{p+1} r_{p+1}}^m e^{-i(E_{r_{p+1}}^m - E_{s_{p+1}}^m) (t-\tilde{\tau}_p)}, \quad (4)$$

where, again, the use of the NRG approximation, implies that this expression should be understood, in general, as being approximate. When $p = n$, Eq. (4) applies for all $t \geq \tilde{\tau}_n$, and can be used to extract the long time limit $t \rightarrow \infty$ of observables, both for a finite or an infinite switch-on time $\tilde{\tau}_n$. Below, we shall discuss the accuracy of the long time limit of observables $O(t \rightarrow \infty)$ as a function of the switch-on time $\tilde{\tau}_n$ (or, equivalently the pulse duration). For zero switch-on time, $\tilde{\tau}_n = 0$ (or equivalently $\tau_1 = \tau_2 = \dots = \tau_p = 0$), the above expression can be converted into that for a single quench³⁶.

For the special case that \hat{O} is the identity operator, $\hat{O} = \hat{I}$, we have

$$1 = \sum_m \sum_{r_1 s_1 \dots r_p s_p r_{p+1} s_{p+1}} S_{r_{p+1} r_p}^m \dots S_{r_2 r_1}^m \rho_m^{i \rightarrow \mathcal{Q}_1}(r_1, s_1) \\ \times e^{-i(E_{r_1}^m - E_{s_1}^m) \tau_1} S_{s_1 s_2}^m \dots e^{-i(E_{r_p}^m - E_{s_p}^m) \tau_p} S_{s_p s_{p+1}}^m. \quad (5)$$

The right hand side of this expression depends on time in a stepwise fashion through the restriction that $t \in [\tilde{\tau}_p, \tilde{\tau}_{p+1})$. The above expression should, in general, be understood as approximate due to the use of the NRG approximation in its derivation. Equation (5) is analogous to the trace of the projected density matrix defined in Refs. 36 and 37, therefore the calculation of $\langle \hat{I} \rangle$ by using this equation will be referred to in the following as the trace of the projected density matrix, and will be denoted by $Tr[\rho^{i \rightarrow f}(t)]$ with $t \in [\tilde{\tau}_p, \tilde{\tau}_{p+1})$. For $t > \tilde{\tau}_n$, it is independent of time and denoted by $Tr[\rho^{i \rightarrow f}(\tilde{\tau}_n)]$. The deviation of $Tr[\rho^{i \rightarrow f}(\tilde{\tau}_n)]$ from 1 represents the cumulative error in the trace due to the NRG approximation and will be investigated in detail in the next section. In the limit of a vanishing switch-on time, equivalent to a single quench, the NRG approximation is inoperative and the resulting expression $1 = Tr[\rho^{i \rightarrow \mathcal{Q}_1}]$ is satisfied exactly, as shown explicitly in Ref. 36.

Since we also wish to compare the present formalism with our previous multiple quench TDNRG formalism, a few words are in order about the latter. In Refs. 36 and 37, we expressed the time evolution of an observable \hat{O} for $t \in [\tilde{\tau}_p, \tilde{\tau}_{p+1})$

as

$$O(t) = \sum_{mrs}^{\epsilon K K'} \rho_{rs}^{i \rightarrow Q_{p+1}}(m, \tilde{\tau}_p) e^{-i(E_r^m - E_s^m)(t - \tilde{\tau}_p)} O_{sr}^m, \quad (6)$$

with $\rho_{rs}^{i \rightarrow Q_{p+1}}(m, \tilde{\tau}_p)$

$$= \sum_e Q_{p+1} \langle rem | e^{-iH^{Q_p} \tau_p} \dots e^{-iH^{Q_1} \tau_1} \rho e^{iH^{Q_1} \tau_1} \dots e^{iH^{Q_p} \tau_p} | sem \rangle_{Q_{p+1}},$$

a projected density matrix depending on each time step $\tilde{\tau}_p$ that was calculated recursively in terms of reduced density matrices and the so called *generalized overlap matrix elements* defined as

$$S_{r_i s_{Q_{p+1}}}^m(\tilde{\tau}_p) \times \delta_{ee'} = \langle rem | e^{iH^{Q_1} \tau_1} \dots e^{iH^{Q_p} \tau_p} | se' m \rangle_{Q_{p+1}}. \quad (7)$$

These generalized overlap matrix elements are also calculated recursively at each time step $\tilde{\tau}_p$ from those at the previous time step $\tilde{\tau}_{p-1}$ and enter in the calculation of the above projected density matrices. In contrast, the formalism presented in this paper evaluates the time evolution in terms of the projected density matrix at the first time step $\rho_m^{i \rightarrow Q_1}(r_1, s_1)$ and the ordinary overlap matrix elements $S_{r_{p+1} s_p}^m$ and bypasses the need for a recursive calculation for quantities entering the expression for $O(t)$. It is therefore numerically more efficient and easier to implement than the approach of Ref. 37. A further difference between the present formalism and that in Refs. 36 and 37 is that in the present formalism only differences of many-body eigenvalues (i.e., excitations) appear in the expression for $O(t)$, whereas in Refs. 36 and 37, absolute eigenvalues (measured relative to an absolute groundstate energy) entered the expressions for the generalized overlap matrix elements. The present formalism therefore avoids the need to explicitly keep track of an absolute ground state energy. Finally, within the multiple quench formalism of Ref. 36 and 37, the limit of infinite switch on time $\tilde{\tau}_n \rightarrow +\infty$ is impossible to take analytically, and that formalism is restricted to numerical evaluations at finite switch-on times. Within the present formalism, on the other hand, it becomes straightforward to take this limit (see Sec. IV). This, in turn, allows for an adiabatic switching of the system between an arbitrary initial state and an arbitrary final state, thereby improving the long time limit of observables.

III. COMPARISON WITH THE PREVIOUS APPROACH

In this section we illustrate the improvement of the present multiple quench TDNRG approach over our previous approach for two specific situations: (i) for the time evolution of the occupation number $\langle n_d(t) \rangle$ in the resonant level model under a square periodic driving of the local level, and, (ii), for the convergence of the long time limit of the occupation number $\langle n_d(t \rightarrow \infty) \rangle$ with respect to increasing the switch on time in the interacting Anderson impurity model following a linear ramp of the local level.

In Fig. 2, we show the error in $Tr[\rho^{i \rightarrow f}(t)]$ versus time and the time evolution of the occupation number in the resonant

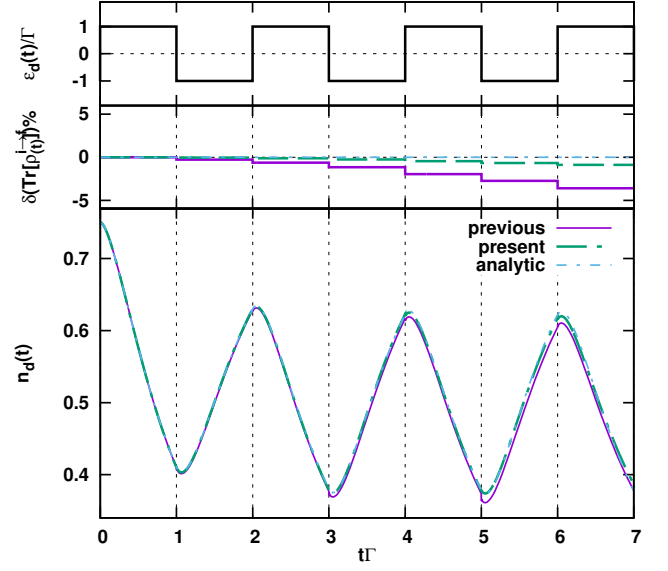


FIG. 2. Results for the resonant level model subject to square periodic driving. Top panel: the square periodic driving used for $\varepsilon_d(t)/\Gamma$, where $\varepsilon_d(t)$ is the local level position and Γ the hybridization strength in the resonant level model. Middle pannel: percentage deviation, $\delta(Tr[\rho^{i \rightarrow f}(t)])$, of the trace of the projected density matrix away from 1 vs $t\Gamma$ in the present approach (dashed line) and the previous multiple-quench approach of Ref. 37 (solid line). The dotted line represents the exact result. Lower panel: Occupation number $n_d(t)$ vs $t\Gamma$ in the present approach (dashed line), the previous approach (solid line), and, in the exact analytic approach (dotted line).

level model (RLM) under a square periodic driving of the local level ε_d from $-\Gamma$ to Γ and back with a period of $2/\Gamma$ (see top panel of Fig. 2). The results of the present approach are compared with those from our previous multiple-quench formalism in Ref. 37 as well as with the exact analytic result for the RLM. From these comparisons, we see that the previous formalism yields a trace for the projected density matrix ($Tr[\rho^{i \rightarrow f}(t)]$) which deviates increasingly away from 1 after each quench. Similarly, the discontinuity in the time evolution of the occupation number at the boundaries of the time steps is clearly visible for times $t\Gamma \gtrsim 5$ in the results from the previous formalism. Within the present formalism, the deviation of $Tr[\rho^{i \rightarrow f}(t)]$ away from 1 is reduced by a factor of more than 10 relative to that in the previous formalism after one period, and the discontinuity in the time evolution of the occupation number also decreases by a similar factor. The present formalism results a time evolution for n_d which is significantly closer to the exact analytic one than that from the previous formalism.

Figure 3 shows results for the Anderson model with a finite Coulomb repulsion U_f in which the system is switched from the mixed valence regime initially ($\varepsilon_d^i = 0$) to the symmetric Kondo regime in the final state ($\varepsilon_d^f = -U_f/2$): in particular, we show the occupation number in the long time limit $n_d(t \rightarrow \infty)$ and the corresponding % error in the trace of the projected density matrix as a function of the switch-on time $\tilde{\tau}_n$, comparing the results also with those from our pre-

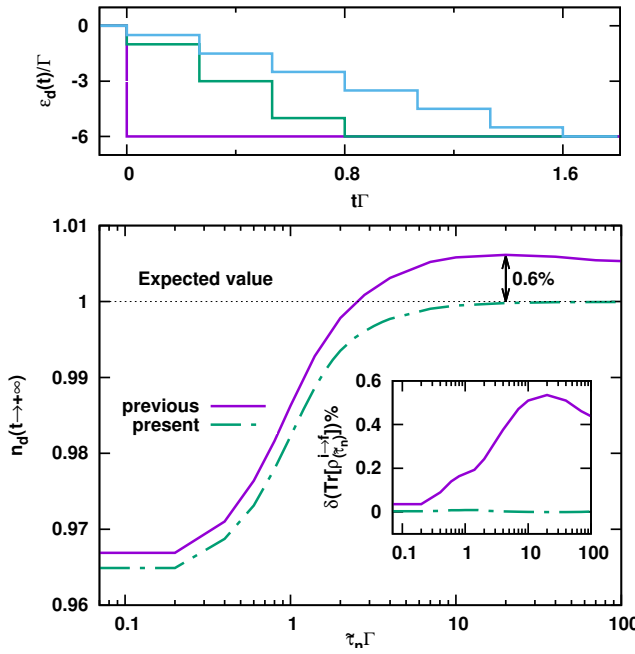


FIG. 3. Results for the Anderson model subject to a linear ramp pulse. Upper panel: the linear ramp pulses used for $\varepsilon_d(t)/\Gamma$ are replaced by the sequences of small quenches depending on the switch-on time, and due to the pulse the system is switched from the mixed valence regime with $\varepsilon_d(t < 0) = 0$ and $U = 12\Gamma$ to the symmetric Kondo regime with $\varepsilon_d(t \geq \tilde{\tau}_n) = -U/2$ and $U = 12\Gamma$ in a time $\tilde{\tau}_n$. Lower panel: The occupation number of the Anderson model in the long time limit $n_d(t \rightarrow \infty)$ vs $\tilde{\tau}_n\Gamma$ in the present approach (dashed line), compared to the approach of Ref. 37 (solid line). For each fixed switch-on time, $\tilde{\tau}_n$, the linear ramp is approximated by a sequence of up to 100 quenches, with the number of quenches chosen such that $n_d(t \rightarrow \infty)$ is converged. The inset shows the corresponding % error in the trace of the projected density matrix $\delta(\text{Tr}[\rho^{i \rightarrow f}(\tilde{\tau}_n)])$ vs $\tilde{\tau}_n\Gamma$ of the present (dashed line) and previous (solid line) multiple-quench approaches.

vious approach. We see that $n_d(t \rightarrow \infty)$ initially increases as the switch-on time increases in both approaches. However, while the occupation number in the previous approach eventually overshoots the expected value of 1 in the final state and only begins to drop to the correct value at very long switch-on times, the present approach converges monotonically to the correct value already at relatively short switch-on times without overshooting. The difference to the expected value at the longest switch-on time $\tilde{\tau}_n\Gamma = 100$ is less than 10^{-4} for the present improved approach. This significant improvement is also observed for the cumulative ($t = \infty > \tilde{\tau}_n$) error in $\text{Tr}[\rho^{i \rightarrow f}(\tilde{\tau}_n)]$. While this is at most $\sim 0.6\%$ in the previous approach, the present formalism yields a value of less than 0.01% in the whole range of switch-on times (see inset to Fig. 3).

In general, then, the present formalism for multiple quenches results in an improved time evolution for observables, including an improved long time limit of observables and smaller discontinuities of observables after each quench. In the next section, we present and discuss the extension of

this formalism to strictly infinite switch-on times.

IV. INFINITE SWITCH-ON TIME AND ACCURATE RESULTS IN THE LONG-TIME LIMIT

In this section, we extend the formalism in Sec. II to the infinite switch-on time limit and apply this to the long time limit of the spectral function and local thermodynamic observables in the interacting Anderson impurity model. We show that the resulting long time limit of the spectral function (Sec. IV A) and local thermodynamic observables (Sec. IV B) approach their expected values in the equilibrium final state to high accuracy. This conclusion is further supported by a (multiple quench) exact diagonalization study of the local level occupation number in the resonant level model (Sec. IV C).

The limit of an infinite switch-on time, $\tilde{\tau}_p \rightarrow +\infty$, can be implemented in Eq. (4) by applying the restriction that $r_1 = s_1$, ..., and $r_p = s_p$, resulting in

$$O(t > \tilde{\tau}_p \rightarrow \infty) = \sum_m \sum_{r_1 \dots r_p r_{p+1} s_{p+1}}^{\notin K_1 \dots K_p K_{p+1} K'_{p+1}} S_{r_{p+1} r_p}^m \dots S_{r_2 r_1}^m \rho_m^{i \rightarrow Q_1}(r_1, r_1) \times S_{r_1 r_2}^m \dots S_{r_p s_{p+1}}^m O_{s_{p+1} r_{p+1}}^m e^{-i(E_{r_{p+1}}^m - E_{s_{p+1}}^m)(t - \tilde{\tau}_p)}. \quad (8)$$

In the long time limit, infinitely long after the last quench, $O(t - \tilde{\tau}_n \rightarrow \infty)$ is calculated by applying the restriction that $r_{n+1} = s_{n+1}$ with $n = p$ to the above equation. Similarly, for the trace of the projected density matrix in the limit $\tilde{\tau}_p \rightarrow +\infty$, we have from Eq. (5)

$$I = \sum_m \sum_{r_1 \dots r_p r_{p+1}}^{\notin K_1 \dots K_p K_{p+1} K'_{p+1}} S_{r_{p+1} r_p}^m \dots S_{r_2 r_1}^m \rho_m^{i \rightarrow Q_1}(r_1, r_1) S_{r_1 r_2}^m \dots S_{r_p r_{p+1}}^m. \quad (9)$$

This equality is not satisfied exactly due to the use of the NRG approximation inherent in its derivation, but as demonstrated in Sec. III, the deviation of the trace from 1 is extremely small. The small error is another reflection of the error in the long time limit of an observable within TDNRG.

A. Application to the long time limit of the spectral function

The general expression for the time-dependent local spectral function $A(\omega, t)$ of the Anderson impurity model for times after the pulse (i.e., for $t > \tilde{\tau}_n$) within the present multiple quench TDNRG approach is derived in Appendix A. We use this here in the limit $\tilde{\tau}_n \rightarrow \infty$ to discuss the long time limit of the spectral function $A(\omega) = A(\omega, t \rightarrow \infty)$.

Figures 4(a)-4(b) show $A(\omega)$ for a system that is gradually driven from, (a), from the uncorrelated symmetric to a correlated symmetric Kondo regime, and, (b), from the mixed valence regime to the symmetric Kondo regime. We use a logarithmic energy axis to focus attention on the long time limit of the low energy Kondo resonance at $|\omega| \lesssim T_K$. For

both switching protocols, we show results for 1, 2, 8 and 32 quenches and also the results expected in the equilibrium final state and the single-quench result obtained by using the self-energy Σ trick⁵⁴. In Fig. 4(a), the single quench result without the self-energy trick has a Kondo resonance which achieves only 60% of its Friedel sum rule value of 1 at $\omega = 0$ ⁵⁵, while the improvement in the single quench result upon using the self-energy trick is not sufficient to reduce the error in the Friedel sum rule to below 20%. In addition, the single quench TDNRG result for spectral functions suffer from additional substructures within the Kondo resonance at $|\omega| \lesssim T_K$, noticeable in Fig. 4(a), and discussed in detail elsewhere³⁹. On the other hand, a real improvement in the low energy Kondo resonance is observed within the multiple quench formalism upon increasing the number of quenches, with 8 quenches already yielding acceptable spectral functions with a less than 10% error in the Friedel sum rule and with 32 quenches yielding highly accurate results approaching the expected value of the spectral function in the equilibrium final state. The substructures are also absent for this number of quenches.

Similar conclusions hold also for the second type of switching shown in Fig. 4(b), in which the system is switched from the mixed valence to the symmetric Kondo regime. An initial particle-hole asymmetry in $A(\omega)$ for the 1, 2, and 8 quench results is eliminated after 32 quenches, restoring the correct symmetry of the final state equilibrium spectral function.

Clearly, the quality of the TDNRG spectral functions at long times, a key input within the scattering states NRG^{32,33}, can be much improved by replacing the single quench TDNRG in Refs. 32 and 33 by the present multiple quench TDNRG. The use of the latter for this purpose should allow, in future, for an accurate study of nonequilibrium steady states for bias voltages on scales of order at least T_K . Furthermore, the high accuracy with which $\text{Tr}[\rho^{i \rightarrow f}(\tilde{\tau}_n)] = 1$ is satisfied in the present formalism (see inset to Fig. 3), guarantees that the spectral sum rule $\int d\omega A(\omega) = 1$ is satisfied to a correspondingly high accuracy.

B. Application to the long time limit of thermodynamic observables

For further insight into the multiple quench TDNRG results, we also look at the results for thermodynamic observables in the long time limit at finite temperatures. The percentage errors of the occupation number and the double occupancy in the long time limit when the system is switched from the asymmetric mixed valence regime to the symmetric Kondo regime are shown in Figs. 5 (a) and 5(b), while the errors in the case of the reverse switching, i.e., from the symmetric Kondo regime to the asymmetric mixed valence regime, are shown in Figs. 5 (c) and 5(d). The percentage error is defined by the relative difference between the expectation value of the local observable in the long time limit and the expected thermodynamic value in the final state, $\delta O(t \rightarrow +\infty) = 100 \times \frac{O(t \rightarrow +\infty) - O_f}{O_f}$. In Fig. 5 (a), the error of the occupation number in the case of a single quench is finite with an extremum at high temperature, and disappears only at

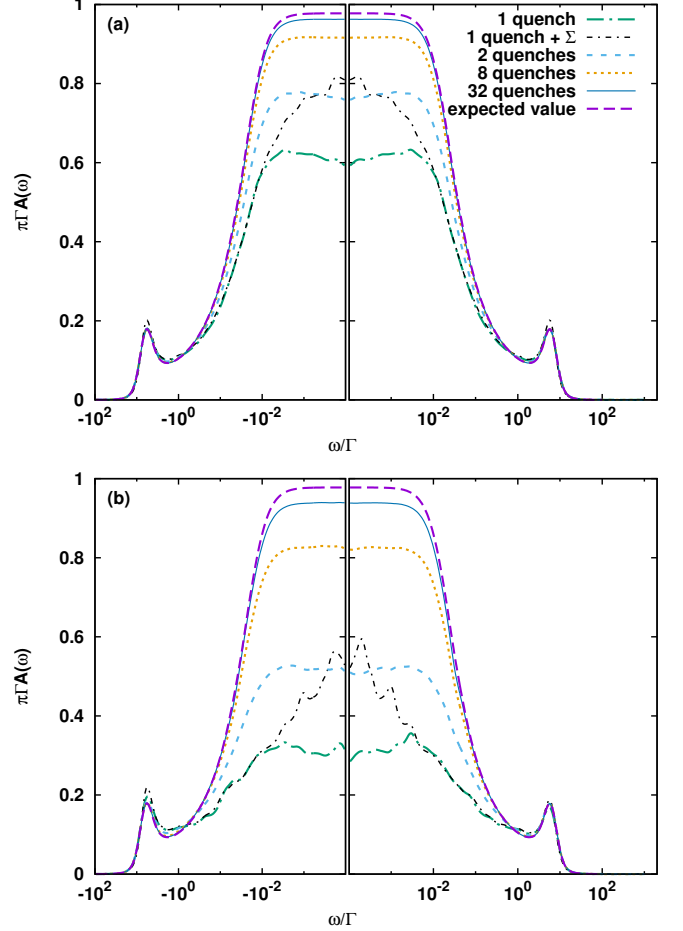


FIG. 4. Normalized spectral function ($\pi\Gamma A(\omega)$) vs normalized frequency ω/Γ in the long-time limit and infinite switch-on time for 2, 8 and 32 quenches compared to that from the single-quench TDNRG with (1 quench + Σ) and without (1 quench) the use of the self-energy⁵⁴. Also shown is the expected value of the spectral function in the equilibrium final state. (a): for switching from the noninteracting with $\epsilon_d^i = U^i = 0$ to the interacting system with $\epsilon_d^f = -U^f/2, U^f = 12\Gamma$. (b): for switching from the asymmetric mixed valence regime with $\epsilon_d^i = 0$ and $U^i = 12\Gamma$ to the symmetric Kondo regime with $\epsilon_d^f = -U^f/2, U^f = 12\Gamma$. $\Gamma = 10^{-3}D$, and $D = 1$ is the half-bandwidth. Calculations were for essentially zero temperature $T = 10^{-4}T_K$, with T_K the Kondo temperature in the final state, NRG parameters: $\Lambda = 4$, $E_{\text{cut}} = 24$, and $N_z = 8$ values for the z-averaging.

the very highest temperature, $T > D$. With a larger number of quenches, 2 and 8, the absolute value of the error significantly decreases at low temperatures $T \leq T_K$, the extrema also decrease in magnitude and remain at around the same temperature as observed in the results for a single quench. In the case of 31 quenches, the error at low temperatures is closer to 0 than in the other cases, and the extremum is also smaller but still finite. In Fig. 5 (b), the error of the double occupancy in the case of single quench is positive at low temperatures $T \lesssim T_K$ and negative at higher temperatures. With an increasing number of quenches, the magnitude of the error

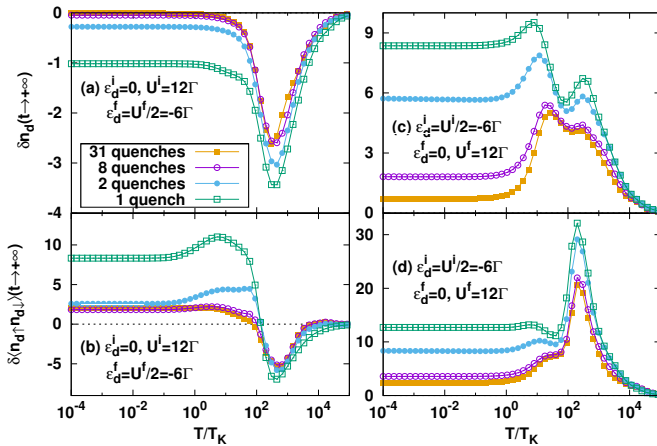


FIG. 5. The percentage error in the expectation value of local observables in the long-time limit vs rescaled temperature T/T_K after a switch from the asymmetric mixed valence to symmetric Kondo regime, (a) and (b), and a switch from the symmetric Kondo regime to the asymmetric mixed valence regime, (c) and (d), with initial and final state parameters shown in the legends. The system is switched by applying 1, 2, 8 or 31 quenches on the local levels, either only ϵ_d in (a) and (b) or both ϵ_d and U in (c) and (d). (a) and (c) show the errors of occupation numbers in the long time limit, (b) and (d) show the errors in the double occupancy. T_K is the Kondo temperature of the symmetric system, $\Gamma = 10^{-3}D$, and $D = 1$ is the half-bandwidth. The calculations are with $\Lambda = 1.6$, the number of kep state $N_s = 900$, and $N_z = 4$ value for the z-averaging.

at $T \lesssim T_K$ is significantly reduced, approaching 0, while the error around the high temperature extremum changes less significantly, and converges to a finite value with increasing number of quenches. In the case of the reverse switching, Figs. 5 (c) and 5(d), the side shoulders at temperatures in the range of $7T_K - 40T_K$ are also observed in addition to the extrema at higher temperature. With an increasing number of quenches, the errors decrease at low temperatures $T \leq T_K$, and the errors around the high-temperature peaks also decrease but still remain finite.

As mentioned in our previous paper³⁶, the error in the long time limit does not only depend on the size of the quench but also on the largest incoherent excitation of the final state, $\epsilon_{inc}^{max} = \max(|\epsilon_f|, |\epsilon_f + U_f|, \Gamma)$. Apparently, the TDNRG calculation for multiple quenches may overcome the first problem of quench size by dividing it into a sequence of smaller ones, but not the second problem since ϵ_{inc}^{max} is the same in both calculations for single quench and multiple quenches. It suggests that the observed extrema at finite temperature may originate from the incoherent excitations.

These results suggest that the TDNRG calculation for multiple quenches systematically improves the long time limit of observables in the low temperature regime $T \leq T_K$, but not in the high temperature regime for temperatures of order the scale of the highest energy incoherent excitation. Nevertheless, the TDNRG presented is promising for the study of the Kondo effect out of equilibrium, where the interest is primarily on low temperatures where a Kondo effect is present, and

on the observed destruction of the Kondo resonance when the bias voltage is increased to values comparable to and above T_K .

C. Exact diagonalization results for the long time limit of thermodynamic observables

Finally, we also present here the results of an exact diagonalization (ED) study for the resonant level model, i.e., the Anderson impurity model with $U = 0$. In the ED calculations, the conduction band is also discretized logarithmically using the parameter Λ as in the NRG calculations, and the resulting model is likewise mapped onto an impurity coupled to a semi-infinite chain. The ED is applied to discrete initial and final state Hamiltonians⁵⁶, and one can then determine from the resulting single particle levels and eigenstates the time evolution of observables following a quench. We have generalized the formulae for the time evolution of observables within this approach, to the case of multiple quenches, and for more details we refer the reader to Appendix C. In the ED calculation, there is no truncation as in the NRG calculation, and one can therefore obtain approximation-free results (no NRG approximation enters). The method can not be applied to the Anderson impurity model with $U \neq 0$, however. Since it also solves the same discrete model as in TDNRG, it can be used as a benchmark to check the TDNRG calculations^{35,56}. In addition, it can be formulated for infinite switch-on times (Appendix C); this allows us to verify that an infinite switch-on time improves the long-time limit of thermodynamic observables, as found in the present multiple quench TDNRG approach.

In Fig. 6, we show the percentage error of the occupation number in the long time limit calculated by ED. The calculation for a single quench in Figs. 6 (a) and 6(b) exhibits the same problem as in the TDNRG calculation. The percentage error is finite and shows an extremum at high temperature. With decreasing Λ in Fig. 6 (a), the error decreases significantly, and the extremum is still located at around the same high temperature. By changing ϵ_d^f in Fig. 6 (b), we can determine the relationship between the extremum at high temperature and the incoherent excitations, as defined above in Sec. IV B. For example, when $\epsilon_d^f = 0\Gamma$, then $\epsilon_{inc}^{max} = \Gamma$, we have that the corresponding extremum appears exactly at $T = \Gamma$. With larger ϵ_d^f , we have $\epsilon_{inc}^{max} = \epsilon_d^f$, and the extremum appears at higher temperatures around ϵ_d^f , but not exactly, due to the interference with the lower energy scale Γ .

Figures 6 (c) and 6(d) show the ED results for multiple quenches with different ϵ_d^f and an infinite switch-on time. With increasing number of quenches, the errors in both figures are reduced close to 0 at low temperature but the errors around the high temperature extremum at $T \approx \epsilon_{inc}^{max} = \epsilon_d^f$ are always finite. In Fig. 6 (c), ϵ_{inc}^{max} equals the lowest energy scale of the final system, then the extrema in the results with different number of quenches are almost the same.

In summary, the ED calculations for both single and multiple quenches without any approximation also show errors in

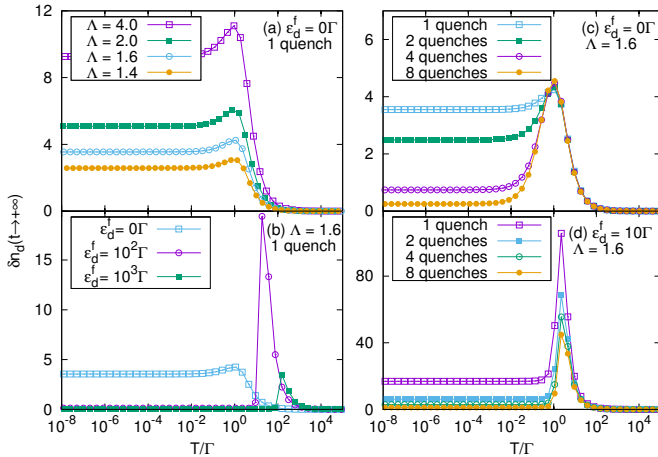


FIG. 6. The percentage error in the expectation value of the occupation number in the long-time limit vs temperature calculated by the exact diagonalization (ED) applied to the resonant level model. a), the ED for single quench is with a fixed final state level position $\varepsilon_d^f = 0$, a fixed quench size, $\Delta\varepsilon_d = \varepsilon_d^f - \varepsilon_d^i = 6\Gamma$, and for different values of Λ . b), the ED is with a fixed Λ and fixed quench size $\Delta\varepsilon_d = 6\Gamma$, and different values of ε_d^f . The ED for multiple quenches with fixed quench size $\Delta\varepsilon_d$ and fixed Λ , with $\varepsilon_d^f = 0\Gamma$ in (c) and with $\varepsilon_d^f = 10\Gamma$ in (d).

the occupation numbers in the long time limit, with extrema at high temperatures as in TDNRG. Dividing a large quench into a sequence of smaller ones with an infinite switch-on time, implemented in the ED calculations presented here, also improves the long time limit of observables at low temperatures as in TDNRG. This further supports the precision of the TDNRG results presented here for infinite switch-on times.

V. CONCLUSIONS

In this paper, we developed an alternative multiple quench TDNRG formalism for general pulses, which reduces further

the effect of the NRG approximation on the time evolution of observables. We showed this by comparison with the previous approach^{36,37}. Specifically, the trace of the projected density matrix versus time remains closer to 1 and the discontinuities in the time evolution of observables following quenches are significantly reduced. Both approaches improve the long time limit of observables for increasing switch on times, i.e. with increasing adiabaticity of the switching from initial to final state. However, the present approach shows a monotonic and faster convergence of the long time limit with increasing switch-on time than the previous approach. Moreover, the present formalism allows the limit of infinite switch on time to be straightforwardly taken analytically, which is impossible in the previous formalism.

We also formulated the spectral function within the new formalism, both for finite and infinite switch on times. For infinite switch on time, we showed that the long time limit of the zero temperature spectral function approached its value in the equilibrium final state with high accuracy: the Friedel sum rule was satisfied to within a few %, which is to be compared with the much larger error of 15% in the single quench approach^{33,39}. Additional features, at $|\omega| \lesssim T_K$, present in the single quench approach³⁹, are absent in the present approach. Hence, the present approach yields accurate results for the long time limit of spectral functions for systems switched between an arbitrary initial and an arbitrary final state. This improvement is important for an accurate description of nonequilibrium steady states of quantum impurity systems, since methods such as the scattering states NRG approach³² for addressing steady states, rely on an accurate time evolved spectral function in the long time limit. In future, we therefore plan to use the present multiple quench formalism to address nonequilibrium steady states in quantum impurity systems.

ACKNOWLEDGMENTS

We acknowledge support by the Deutsche Forschungsgemeinschaft via RTG 1995 and supercomputer support by the John von Neumann institute for Computing (Jülich).

Appendix A: Spectral function in the long time limit

In order to evaluate the spectral function, we require an expression for the retarded two-time Green function $G_{BC}(t + t', t) = -i\theta(t') \text{Tr}\{\hat{\rho}[\hat{B}(t + t'), \hat{C}(t)]_s\}$ within TDNRG. Since we are here only interested in the long-time limit after the last quench, $t + t' > t > \tilde{\tau}_n$, we can write

$$\begin{aligned}
 G_{BC}(t + t', t) &= -i\theta(t') \text{Tr}\{\hat{\rho}[\hat{B}(t + t'), \hat{C}(t)]_s\} \\
 &= -i\theta(t') \text{Tr}\{\hat{\rho}[e^{iH^f(t+t'-\tilde{\tau}_n)} \dots e^{iH^{\mathcal{Q}_1}\tau_1} \hat{B} e^{-iH^{\mathcal{Q}_1}\tau_1} \dots e^{-iH^f(t+t'-\tilde{\tau}_n)}, e^{iH^f(t-\tilde{\tau}_n)} \dots e^{iH^{\mathcal{Q}_1}\tau_1} \hat{C} e^{-iH^{\mathcal{Q}_1}\tau_1} \dots e^{-iH^f(t-\tilde{\tau}_n)}]_s\} \\
 &= -i\theta(t') \text{Tr}\{e^{-iH^f(t-\tilde{\tau}_n)} \dots e^{-iH^{\mathcal{Q}_1}\tau_1} \hat{\rho} e^{iH^{\mathcal{Q}_1}\tau_1} \dots e^{iH^f(t-\tilde{\tau}_n)} [e^{iH^f t'} \hat{B} e^{-iH^f t'}, \hat{C}]_s\}
 \end{aligned} \tag{A1}$$

Inserting decompositions of unity $1 = \sum_{lem} |lem\rangle\langle lem|$ in the above gives,

$$G_{BC}(t + t', t) = -i\theta(t') \sum_{\substack{lem \\ l'e'm' \\ l'e''m'}} \sum_{\substack{l_1 e_1 m_1 \\ l'_1 e'_1 m'_1 \\ l''_1 e''_1 m''_1}} \dots \sum_{\substack{l_n e_n m_n \\ l'_n e'_n m'_n \\ l''_n e''_n m''_n}} {}_f\langle lem| e^{-iH^f(t-\tilde{\tau}_n)} e^{-iH^{Q_n}\tau_n} |l_n e_n m_n\rangle_{Q_n} \dots {}_{Q_2}\langle l_2 e_2 m_2| e^{-iH^{Q_1}\tau_1} |l_1 e_1 m_1\rangle_{Q_1} \\ \times {}_{Q_1}\langle l_1 e_1 m_1| \hat{\rho}|l'_1 e'_1 m'_1\rangle_{Q_1} {}_{Q_1}\langle l'_1 e'_1 m'_1| e^{iH^{Q_1}\tau_1} |l'_2 e'_2 m'_2\rangle_{Q_2} \dots {}_{Q_n}\langle l'_n e'_n m'_n| e^{iH^{Q_n}\tau_n} e^{iH_f(t-\tilde{\tau}_n)} |l'' e'' m''\rangle_f \\ \times {}_f\langle l'' e'' m''| e^{iH^f t'} \hat{B} e^{-iH^f t'} |l'' e'' m''\rangle_f {}_f\langle l'' e'' m''| \hat{C} |lem\rangle_f + {}_f\langle l'' e'' m''| \hat{C} |l'' e'' m''\rangle_f {}_f\langle l'' e'' m''| e^{iH^f t'} \hat{B} e^{-iH^f t'} |lem\rangle_f \quad (\text{A2})$$

Converting the multiple-shell summations over discarded states into a shell-diagonal restricted sum⁵³ leads to

$$G_{BC}(t + t', t) = -i\theta(t') \sum_m \sum_{\substack{\#KK'K''K_1K'_1\dots K_nK'_n \\ rsqr_1s_1\dots r_n s_n}} S_{rr_n}^m \dots S_{r_2r_1}^m \rho_m^{i\rightarrow Q_1}(r_1, s_1) e^{-i(E_{r_1}^m - E_{s_1}^m)\tau_1} S_{s_1s_2}^m \dots e^{-i(E_{r_n}^m - E_{s_n}^m)\tau_n} S_{s_ns}^m e^{-i(E_r^m - E_s^m)(t - \tilde{\tau}_n)} \\ \times (B_{sq}^m e^{i(E_s^m - E_q^m)t'} C_{qr}^m + C_{sq}^m B_{qr}^m e^{i(E_q^m - E_r^m)t'}). \quad (\text{A3})$$

Fourier transforming this Green function with respect to the time difference t' results in

$$G_{BC}(\omega, t) = \sum_m \sum_{\substack{\#KK'K''K_1K'_1\dots K_nK'_n \\ rsqr_1s_1\dots r_n s_n}} S_{rr_n}^m \dots S_{r_2r_1}^m \rho_m^{i\rightarrow Q_1}(r_1, s_1) e^{-i(E_{r_1}^m - E_{s_1}^m)\tau_1} S_{s_1s_2}^m \dots e^{-i(E_{r_n}^m - E_{s_n}^m)\tau_n} S_{s_ns}^m e^{-i(E_r^m - E_s^m)(t - \tilde{\tau}_n)} \\ \times \left(\frac{B_{sq}^m C_{qr}^m}{\omega + E_s^m - E_q^m + i\eta} + \frac{C_{sq}^m B_{qr}^m}{\omega + E_q^m - E_r^m + i\eta} \right). \quad (\text{A4})$$

Then we have the spectral function, $A(\omega, t) = -\text{Im}[G(\omega, t)]/\pi$, at the long time limit $t - \tilde{\tau}_n \rightarrow +\infty$ with finite $\tau_{p=1,\dots,n}$

$$A(\omega, t) = \sum_m \sum_{\substack{\#KK'K_1K'_1\dots K_nK'_n \\ rqr_1s_1\dots r_n s_n}} S_{rr_n}^m \dots S_{r_2r_1}^m \rho_m^{i\rightarrow Q_1}(r_1, s_1) e^{-i(E_{r_1}^m - E_{s_1}^m)\tau_1} S_{s_1s_2}^m \dots e^{-i(E_{r_n}^m - E_{s_n}^m)\tau_n} S_{s_ns}^m \\ \times [B_{rq}^m C_{qr}^m \delta(\omega + E_r^m - E_q^m) + C_{sq}^m B_{qr}^m \delta(\omega + E_q^m - E_r^m)], \quad (\text{A5})$$

and the long time limit with $\tau_{p=1,\dots,n} \rightarrow +\infty$

$$A(\omega, t) = \sum_m \sum_{\substack{\#KK'K_1\dots K_n \\ rqr_1\dots r_n}} S_{rr_n}^m \dots S_{r_2r_1}^m \rho_m^{i\rightarrow Q_1}(r_1, r_1) S_{r_1r_2}^m \dots S_{r_nr_n}^m [B_{rq}^m C_{qr}^m \delta(\omega + E_r^m - E_q^m) + C_{sq}^m B_{qr}^m \delta(\omega + E_q^m - E_r^m)]. \quad (\text{A6})$$

Appendix B: Spectral function in the long time limit: dependence on finite switch-on time

We show in Fig. 7 the dependence of the long time limit of the spectral function $A(\omega) = A(\omega, t \rightarrow \infty)$ on the switch-on time $\tau = \tilde{\tau}_n$. As with the occupation number, the long time limit of the spectral function also improves and approaches the expected value in the equilibrium final state with increasing switch-on time τ . In the case of switching from the asymmetric to symmetric Kondo regime, Fig. 4 (b), the spectral function in the long time limit becomes more symmetric with increasing τ . However, the spectral function shows small additional structures at $|\omega| < T_K$ even when the switch-on time τ exceeds the time scale $1/T_K$ for the formation of the Kondo resonance³⁹. The error in the spectral sum rule $\int_{-\infty}^{+\infty} d\omega A(\omega, t \rightarrow \infty) = 1$ is violated in this case by 0.1%. This is attributed to the NRG approximation in the multiple quench formalism, which results in a cumulative error in the trace of the projected density matrix and a discontinuity in the

time evolution of observables, as discussed in Sec. III. In the case of switching from a noninteracting to an interacting system, Fig. 4 (a), the long time limit of the spectral function lies closer to the expected result than that for the second switching protocol in Fig. 4 (b) for each τ . However, at the longest τ , additional structures within the Kondo resonance at $|\omega| < T_K$ are still visible and due to the use of NRG approximation for finite switch-on times. The above findings support the conclusion that accurate results can be obtained for the long time limit of the spectral function within TDNRG by replacing a single large quench by a sequence of smaller quenches and switching the system slowly from one state to the other (i.e., with increasing τ).

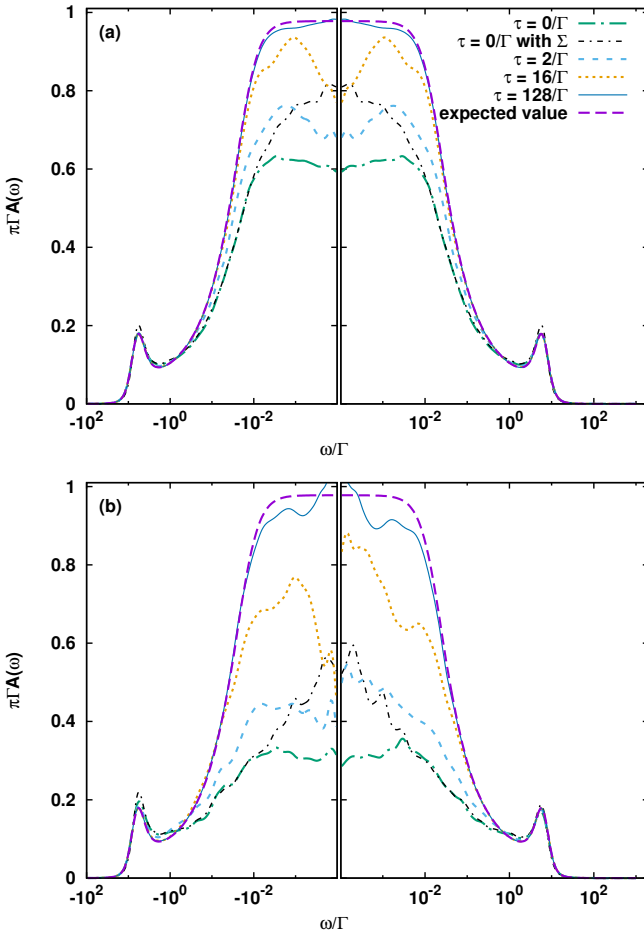


FIG. 7. Spectral function in the long-time limit $A(\omega, t \rightarrow \infty)$ vs ω/Γ for different finite switch-on times $\tau = \tau_n$. Also shown is the expected equilibrium spectral function in the final state. (a) Switching from a noninteracting regime with $\epsilon_d^i = 0$ and $U^i = 0$ to an interacting Kondo regime with $\epsilon_d^f = -U^f/2$ and $U^f = 12\Gamma$. (b) Switching from the asymmetric mixed valence regime with $\epsilon_d^i = 0$ and $U^i = 12\Gamma$ to the symmetric Kondo regime with $\epsilon_d^f = -U^f/2$ and $U^f = 12\Gamma$. $\Gamma = 10^{-3}D$, with $D = 1$ the half-bandwidth. Calculations were for essentially zero temperature, $T = 10^{-4}T_K$, with T_K the Kondo temperature in the final state. NRG parameters: $\Lambda = 5$, $E_{\text{cut}} = 24$, and $N_z = 8$ values for the z-averaging.

Appendix C: Exact diagonalization of the resonant level model with multiple quenches

The real-time evolution of a system, modeled by the resonant level model (RLM), following a single quench can be calculated via exact diagonalization (ED)⁵⁶. In this appendix, we derive results for the time dependence of the occupation number of the resonant level model, $\langle n_d(t) \rangle$, and also for the time dependence of the conduction electron orbital occupation numbers, first for the case of two quenches, and then generalizing this to the case of an arbitrary number of quenches. The presented expressions are then free of any approximations, both for finite and infinite switch-on times.

In the ED of the RLM, the conduction band is also dis-

cretized with the parameter Λ and mapped onto a Wilson chain as in the NRG calculation. Then we have the following discrete model,

$$H_N(t) = \epsilon_d(t)d^\dagger d + V(t)(d^\dagger c_0 + c_0^\dagger d) + \sum_{n=0}^{N-2} t_n(c_n^\dagger c_{n+1} + c_{n+1}^\dagger c_n) \\ = \vec{a}^\dagger M(t) \vec{a}, \quad (C1)$$

with $\vec{a} = \begin{pmatrix} d \\ c_0 \\ \vdots \end{pmatrix}$, $\vec{a}^\dagger = (d^\dagger \ c_0^\dagger \ \dots)$, and

$$M(t) = \begin{pmatrix} \epsilon_d(t) & V & 0 & 0 \\ V & 0 & t_0 & 0 \\ 0 & t_0 & 0 & \ddots \\ 0 & 0 & \ddots & \ddots \end{pmatrix}. \quad (C2)$$

$M(t)$ can be diagonalized as follows

$$M(t) = U(t)^\dagger \text{diag}(\epsilon_1(t), \epsilon_2(t), \dots) U(t). \quad (C3)$$

$H(t)$ is represented in Fig. 8, in which each Hamiltonian can

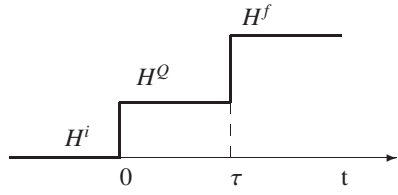


FIG. 8. A system driven from the initial H^i to the final state H^f via the intermediate state described by $\{H^Q\}$.

be expressed in the diagonal form as $H^i = \sum_n \epsilon_n^i f_n^{i\dagger} f_n^i$, $H^Q = \sum_n \epsilon_n^Q f_n^Q f_n^Q$, and $H^f = \sum_n \epsilon_n^f f_n^{f\dagger} f_n^f$ with

$$f_n^i = \sum_l U_{nl}^i \alpha_l, \quad f_n^Q = \sum_l U_{nl}^Q \alpha_l, \quad f_n^f = \sum_l U_{nl}^f \alpha_l \quad (C4)$$

$$f_n^{i\dagger} = \sum_l \alpha_l^\dagger U_{nl}^{i\dagger}, \quad f_n^{Q\dagger} = \sum_l \alpha_l^\dagger U_{nl}^{Q\dagger}, \quad f_n^{f\dagger} = \sum_l \alpha_l^\dagger U_{nl}^{f\dagger}. \quad (C5)$$

The operator for the occupation number of site m is defined as

$$n_m = \alpha_m^\dagger \alpha_m = \begin{cases} d^\dagger d & m = 0; \\ c_{m-1}^\dagger c_{m-1} & m > 1. \end{cases} \quad (C6)$$

The expectation value of the occupation number is given by

$$\langle n_m(t > \tau) \rangle = \text{Tr}[\rho(t)n_m], \quad (C7)$$

with $\rho(t) = e^{-iH^f(t-\tau)} e^{-iH^Q\tau} \rho_0 e^{iH^Q\tau} e^{iH^f(t-\tau)}$ and $\rho_0 = \frac{e^{-\beta H^i}}{Z} = \frac{e^{-\beta \sum_n \epsilon_n^i f_n^{i\dagger} f_n^i}}{\text{Tr}[e^{-\beta \sum_n \epsilon_n^i f_n^{i\dagger} f_n^i}]}.$ Then we have

$$\langle n_m(t > \tau) \rangle = \text{Tr}[e^{-iH^f(t-\tau)} e^{-iH^Q\tau} \rho_0 e^{iH^Q\tau} e^{iH^f(t-\tau)} n_m] \\ = \text{Tr}[e^{-iH^Q\tau} \rho_0 e^{iH^Q\tau} \underbrace{e^{iH^f(t-\tau)} n_m e^{-iH^f(t-\tau)}}_{n_m(t-\tau)}]. \quad (C8)$$

$$\begin{aligned}
n_m(t-\tau) &= e^{iH^f(t-\tau)} \underbrace{\alpha_m^\dagger \alpha_m}_{n_m} e^{-iH^f(t-\tau)} \\
&= \sum_{nn'} e^{iH^f(t-\tau)} f_n^{f\dagger} f_{n'}^f e^{-iH^f(t-\tau)} U_{nm}^f U_{mn'}^{f\dagger} \\
&= \sum_{nn'} \underbrace{e^{iH^f(t-\tau)} f_n^{f\dagger} e^{-iH^f(t-\tau)}}_{f_n^{f\dagger}(t-\tau)} \underbrace{e^{iH^f(t-\tau)} f_{n'}^f e^{-iH^f(t-\tau)}}_{f_{n'}^f(t-\tau)} U_{nm}^f U_{mn'}^{f\dagger} \\
&= \sum_{nn'} e^{i(\epsilon_n^f - \epsilon_{n'}^f)(t-\tau)} f_n^{f\dagger} f_{n'}^f U_{nm}^f U_{mn'}^{f\dagger}, \tag{C9}
\end{aligned}$$

since $\partial_{(t-\tau)} f_n^f(t-\tau) = i[H^f, f_n^f(t-\tau)] = -i\epsilon_n^f f_n^f(t-\tau)$, then $f_n^f(t-\tau) = e^{-i\epsilon_n^f(t-\tau)} f_n^f$. Substituting C9 into C8, we have

$$\begin{aligned}
\langle n_m(t > \tau) \rangle &= \sum_{nn'} e^{i(\epsilon_n^f - \epsilon_{n'}^f)(t-\tau)} \text{Tr}[e^{-iH^Q\tau} \rho_0 e^{iH^Q\tau} f_n^{f\dagger} f_{n'}^f] U_{nm}^f U_{mn'}^{f\dagger} \\
&= \sum_{nn'} e^{i(\epsilon_n^f - \epsilon_{n'}^f)(t-\tau)} \sum_{kk'} \text{Tr}[e^{-iH^Q\tau} \rho_0 e^{iH^Q\tau} f_k^{Q\dagger} f_{k'}^Q] \\
&\quad \times (U^Q U^{f\dagger})_{kn} (U^f U^{Q\dagger})_{n'k'} U_{nm}^f U_{mn'}^{f\dagger}. \tag{C10}
\end{aligned}$$

Similarly, the trace in C10 is evaluated as follows

$$\begin{aligned}
&\text{Tr}[e^{-iH^Q\tau} \rho_0 e^{iH^Q\tau} f_k^{Q\dagger} f_{k'}^Q] \\
&= \text{Tr}[\rho_0 e^{iH^Q\tau} f_k^Q e^{-iH^Q\tau} e^{iH^Q\tau} f_{k'}^Q e^{-iH^Q\tau}] \\
&= e^{i(\epsilon_k^Q - \epsilon_{k'}^Q)\tau} \text{Tr}[\rho_0 f_k^{Q\dagger} f_{k'}^Q] \\
&= e^{i(\epsilon_k^Q - \epsilon_{k'}^Q)\tau} \sum_{qq'} \underbrace{\text{Tr}[\rho_0 f_q^{i\dagger} f_{q'}^i]}_{f(\epsilon_q^i)\delta_{qq'}} (U^i U^{Q\dagger})_{qk} (U^Q U^{i\dagger})_{k'q'} \\
&= e^{i(\epsilon_k^Q - \epsilon_{k'}^Q)\tau} \sum_q f(\epsilon_q^i) (U^i U^{Q\dagger})_{qk} (U^Q U^{i\dagger})_{k'q}, \tag{C11}
\end{aligned}$$

in which $f(\epsilon_q^i)$ is the Fermi-Dirac distribution. Substituting C11 into C10, we have

$$\begin{aligned}
\langle n_m(t > \tau) \rangle &= \sum_{nn'} e^{i(\epsilon_n^f - \epsilon_{n'}^f)(t-\tau)} \sum_{kk'} e^{i(\epsilon_k^Q - \epsilon_{k'}^Q)\tau} \sum_q f(\epsilon_q^i) (U^i U^{Q\dagger})_{qk} (U^Q U^{i\dagger})_{k'q} \\
&\quad \times (U^Q U^{f\dagger})_{kn} (U^f U^{Q\dagger})_{n'k'} U_{nm}^f U_{mn'}^{f\dagger}. \tag{C12}
\end{aligned}$$

Defining

$$n_{kk'}^{i \rightarrow Q} = \sum_q f(\epsilon_q^i) (U^i U^{Q\dagger})_{qk} (U^Q U^{i\dagger})_{k'q} \tag{C13}$$

$$n_{nn'}^{i \rightarrow f} = \sum_{kk'} e^{i(\epsilon_k^Q - \epsilon_{k'}^Q)\tau} n_{kk'}^{i \rightarrow Q} (U^Q U^{f\dagger})_{kn} (U^f U^{Q\dagger})_{n'k'}, \tag{C14}$$

we have

$$\langle n_m(t > \tau) \rangle = \sum_{nn'} e^{i(\epsilon_n^f - \epsilon_{n'}^f)(t-\tau)} n_{nn'}^{i \rightarrow f} U_{nm}^f U_{mn'}^{f\dagger}. \tag{C15}$$

These expressions are generalized to the case of $(p+1)$ quenches as follows

$$n_{nn'}^{i \rightarrow f} = \sum_{kk'} e^{i(\epsilon_k^{Q_p} - \epsilon_{k'}^{Q_p})\tau_p} n_{kk'}^{i \rightarrow Q_p} (U^{Q_p} U^{f\dagger})_{kn} (U^f U^{Q_p\dagger})_{n'k'}, \tag{C16}$$

which is a recursion relation allowing $n^{i \rightarrow Q_p}$ to be derived from $n^{i \rightarrow Q_{p-1}}$, and consequently from $n^{i \rightarrow Q_1}$ determined in C13. Finally, we have for the occupation of the orbitals

$$\langle n_m(t > \tilde{\tau}_p) \rangle = \sum_{nn'} e^{i(\epsilon_n^f - \epsilon_{n'}^f)(t-\tilde{\tau}_p)} n_{nn'}^{i \rightarrow f} U_{nm}^f U_{mn'}^{f\dagger}, \tag{C17}$$

with $\tilde{\tau}_p = \sum_{i=1}^p \tau_i$.

The formulae above for the real-time dynamics following multiple quenches within ED is without any approximation. The extension to the case of an infinite switch-on time, $\tilde{\tau}_p \rightarrow +\infty$, is obtained straight forwardly by setting $k = k'$ in C16, and yields the time independent long-time limit result for the occupation numbers.

¹ D. C. Langreth and P. Nordlander, *Phys. Rev. B* **43**, 2541 (1991).
² M. Pamperin, F. X. Bronold, and H. Fehske, *Phys. Rev. B* **91**, 035440 (2015).
³ A.-P. Jauho, N. S. Wingreen, and Y. Meir, *Phys. Rev. B* **50**, 5528 (1994).
⁴ E. Sela and Y. Oreg, *Phys. Rev. Lett.* **96**, 166802 (2006).
⁵ A. Schiller and A. Silva, *Phys. Rev. B* **77**, 045330 (2008).
⁶ J. Splettstoesser, M. Governale, J. König, and R. Fazio, *Phys. Rev. Lett.* **95**, 246803 (2005).
⁷ L. Perfetti, P. A. Loukakos, M. Lisowski, U. Bovensiepen, H. Berger, S. Biermann, P. S. Cornaglia, A. Georges, and M. Wolf, *Phys. Rev. Lett.* **97**, 067402 (2006).
⁸ J. K. Freericks, V. M. Turkowski, and V. Zlatić, *Phys. Rev. Lett.* **97**, 266408 (2006).

⁹ J. K. Freericks, H. R. Krishnamurthy, and T. Pruschke, *Phys. Rev. Lett.* **102**, 136401 (2009).
¹⁰ H. Aoki, N. Tsuji, M. Eckstein, M. Kollar, T. Oka, and P. Werner, *Rev. Mod. Phys.* **86**, 779 (2014).
¹¹ J. Bauer, C. Salomon, and E. Demler, *Phys. Rev. Lett.* **111**, 215304 (2013).
¹² Y. Nishida, *Phys. Rev. Lett.* **111**, 135301 (2013).
¹³ Y. Nishida, *Phys. Rev. A* **93**, 011606 (2016).
¹⁴ L. Rieger, N. Darkwah Oppong, M. Höfer, D. Rio Fernandes, I. Bloch, and S. Fölling, ArXiv e-prints (2017), [arXiv:1708.03810](https://arxiv.org/abs/1708.03810).
¹⁵ M. Cetina, M. Jag, R. S. Lous, I. Fritzsche, J. T. M. Walraven, R. Grimm, J. Levinsen, M. M. Parish, R. Schmidt, M. Knap, and E. Demler, *Science* **354**, 96 (2016).

¹⁶ W. Metzner, M. Salmhofer, C. Honerkamp, V. Meden, and K. Schönhammer, *Rev. Mod. Phys.* **84**, 299 (2012).

¹⁷ D. M. Kennes, S. G. Jakobs, C. Karrasch, and V. Meden, *Phys. Rev. B* **85**, 085113 (2012).

¹⁸ H. Schoeller, *The European Physical Journal Special Topics* **168**, 179 (2009).

¹⁹ D. Lobaskin and S. Kehrein, *Phys. Rev. B* **71**, 193303 (2005).

²⁰ P. Wang and S. Kehrein, *Phys. Rev. B* **82**, 125124 (2010).

²¹ G. Cohen, E. Gull, D. R. Reichman, and A. J. Millis, *Phys. Rev. Lett.* **112**, 146802 (2014).

²² E. Gull, A. J. Millis, A. I. Lichtenstein, A. N. Rubtsov, M. Troyer, and P. Werner, *Rev. Mod. Phys.* **83**, 349 (2011).

²³ U. Weiss, *Quantum dissipative systems*, Vol. 13 (World Scientific Pub Co Inc, 2008).

²⁴ L. Mühlbacher and E. Rabani, *Phys. Rev. Lett.* **100**, 176403 (2008).

²⁵ A. J. Daley, C. Kollath, U. Schollwöck, and G. Vidal, *Journal of Statistical Mechanics: Theory and Experiment* **2004**, P04005 (2004).

²⁶ S. R. White and A. E. Feiguin, *Phys. Rev. Lett.* **93**, 076401 (2004).

²⁷ P. Schmitteckert, *Journal of Physics Conference Series* **220**, 012022 (2010).

²⁸ C. Schinabeck, A. Erpenbeck, R. Härtle, and M. Thoss, *Phys. Rev. B* **94**, 201407 (2016).

²⁹ C. Schinabeck, R. Härtle, and M. Thoss, ArXiv e-prints (2018), arXiv:1802.09283 [cond-mat.mes-hall].

³⁰ F. B. Anders and A. Schiller, *Phys. Rev. Lett.* **95**, 196801 (2005).

³¹ F. B. Anders and A. Schiller, *Phys. Rev. B* **74**, 245113 (2006).

³² F. B. Anders, *Phys. Rev. Lett.* **101**, 066804 (2008).

³³ F. B. Anders, *Journal of Physics-Condensed Matter* **20**, 195216 (2008).

³⁴ E. Eidelstein, A. Schiller, F. Gütge, and F. B. Anders, *Phys. Rev. B* **85**, 075118 (2012).

³⁵ F. Gütge, F. B. Anders, U. Schollwöck, E. Eidelstein, and A. Schiller, *Phys. Rev. B* **87**, 115115 (2013).

³⁶ H. T. M. Nghiem and T. A. Costi, *Phys. Rev. B* **89**, 075118 (2014).

³⁷ H. T. M. Nghiem and T. A. Costi, *Phys. Rev. B* **90**, 035129 (2014).

³⁸ H. T. M. Nghiem, D. M. Kennes, C. Klöckner, V. Meden, and T. A. Costi, *Phys. Rev. B* **93**, 165130 (2016).

³⁹ H. T. M. Nghiem and T. A. Costi, *Phys. Rev. Lett.* **119**, 156601 (2017).

⁴⁰ A. Khedri, T. A. Costi, and V. Meden, *Phys. Rev. B* **96**, 195155 (2017).

⁴¹ A. Rosch, *The European Physical Journal B-Condensed Matter and Complex Systems* **85**, 6 (2012).

⁴² K. G. Wilson, *Rev. Mod. Phys.* **47**, 773 (1975).

⁴³ H. R. Krishna-murthy, J. W. Wilkins, and K. G. Wilson, *Phys. Rev. B* **21**, 1003 (1980).

⁴⁴ C. Gonzalez-Buxton and K. Ingersent, *Phys. Rev. B* **57**, 14254 (1998).

⁴⁵ R. Bulla, T. A. Costi, and T. Pruschke, *Rev. Mod. Phys.* **80**, 395 (2008).

⁴⁶ G. D. Scott, Z. K. Keane, J. W. Ciszek, J. M. Tour, and D. Natelson, *Phys. Rev. B* **79**, 165413 (2009).

⁴⁷ A. V. Kretinin, H. Shtrikman, D. Goldhaber-Gordon, M. Haml, A. Weichselbaum, J. von Delft, T. Costi, and D. Mahalu, *Phys. Rev. B* **84**, 245316 (2011).

⁴⁸ G. D. Scott, D. Natelson, S. Kirchner, and E. Muñoz, *Phys. Rev. B* **87**, 241104 (2013).

⁴⁹ A. Oguri and A. C. Hewson, *Phys. Rev. B* **97**, 035435 (2018).

⁵⁰ A. Weichselbaum and J. von Delft, *Phys. Rev. Lett.* **99**, 076402 (2007).

⁵¹ W. C. Oliveira and L. N. Oliveira, *Phys. Rev. B* **49**, 11986 (1994).

⁵² V. L. Campo and L. N. Oliveira, *Phys. Rev. B* **72**, 104432 (2005).

⁵³ Equation (D4) in Weymann *et al*⁵⁷.

⁵⁴ R. Bulla, A. C. Hewson, and T. Pruschke, *Journal of Physics: Condensed Matter* **10**, 8365 (1998).

⁵⁵ The Friedel sum rule⁵⁸ states that $\pi\Gamma A(\omega = 0) = \sin^2(\pi n_d/2)$ where $A(\omega)$ is the zero temperature spectral function. For a particle-hole symmetric final state, the RHS equals 1.

⁵⁶ F. Gütge, *Real time dynamics and critical phenomena of quantum impurity systems*, Ph.D. thesis, University of Dortmund (2013).

⁵⁷ I. Weymann, J. von Delft, and A. Weichselbaum, *Phys. Rev. B* **92**, 155435 (2015).

⁵⁸ A. C. Hewson, *The Kondo Problem to Heavy Fermions* (Cambridge University Press, Cambridge, 1997).